Attitude Determination and Control System of the ORCASat

Bernardo Lúcio de Melo Sabino
bernardo.sabino@tecnico.ulisboa.pt

Instituto Superior Técnico, Lisboa, Portugal

September 2020

Abstract

The goal of this article is to present the results and conclusions of an Attitude Determination and Control System (ADCS) capable of achieving the mission requirements of the ORCASat, a 2U CubeSat: Ability to detumble the satellite from high initial angular velocities; Guarantee a pointing error smaller than 10°; And guarantee an attitude estimation error smaller than 2°. The active ADCS control is provided by magnetorquers while a momentum wheel is used for passive attitude stabilization. Four different attitude control algorithms, the Constant Gain Controller, the Finite Horizon Controller, the Infinite Horizon Controller, and the Sliding Mode Controller, were tested and compared in terms of efficiency and pointing accuracy. The best performing algorithm was selected, and its performance was analyzed under different scenarios, including model uncertainties. In order to detumble the spacecraft, a modified B-dot controller was implemented. Its performance was tested under different conditions. The ORCASat's attitude sensor suite includes four sun sensors, a magnetometer, and a gyroscope. The Quaternion Estimator (QUEST) algorithm was implemented to initialize the main attitude estimator, the Multiplicative Extended Kalman Filter (MEKF). A real-time magnetometer calibration filter, the Magnetometer Calibration Extended Kalman Filter, was implemented and studied as an attempt to improve the performance of the MEKF. Different cases were devised to analyze the performance of these algorithms. All the simulations were performed under a realistic Matlab/Simulink environment. The different simulations showed that the proposed ADCS could fulfill the mission requirements, even with the existence of model uncertainties.

Keywords: ADCS, CubeSat, attitude determination, attitude control, magnetometer calibration, magnetorquer

1. Introduction

A CubeSat is a square-shaped miniature satellite built to standard dimensions (Units or "U") of 10cm × 10cm × 10cm, with a mass of up to 1.33kg per U [1]. A CubeSat can be used alone (1U) or in groups of multiple units, originating 2U, 3U, 6U, up to a maximum 24U. Although CubeSats were initially developed as an educational tool, they are increasingly being put to active use in orbit for technology demonstration, scientific studies, and even commercial purposes. The small size of these satellites presents some challenges for the design of the Attitude Determination and Control System (ADCS) since these satellites are very limited not only in terms of mass and volume, but they must also obey to strict power and cost limitations.

The purpose of this paper is to present and evaluate the efficiency of a fully conceptualized ADCS under the framework of the Optical and Radio Calibration Satellite (ORCASat). The ORCASat is part of the Canadian CubeSat Project and is being developed through a combined effort between teams at the University of British Columbia, Simon Fraser University, the University of Victoria (British Columbia, Canada), and Instituto Superior Técnico (Lisbon, Portugal). The proposed ADCS must obey the three mission requirements: Ability to detumble the spacecraft; Guarantee an attitude knowledge error smaller than 2°; And guarantee a pointing error smaller than 10°. These requirements must be guaranteed for the full orbit independently if the CubeSat is in eclipse or in sunlit. The ADCS of the ORCASat features a sensor suite composed of a 3D digital magnetometer and gyroscope, four digital sun sensors, and a GNSS receiver. The active ADCS control is provided by three orthogonal magnetorquers while a momentum wheel is used for passive attitude stabilization.

2. Background

2.1. Reference Frames

The Earth-Centered Inertial (ECI) frame, here designated by $I = \{\hat{\mathbf{i}}_1, \hat{\mathbf{i}}_2, \hat{\mathbf{i}}_3\}$, is an approximate inertial frame whose origin is in the center of mass of the Earth. The $\hat{\mathbf{i}}_3$ axis is aligned with the Earth's North pole, and the $\hat{\mathbf{i}}_1$ axis is aligned with the *ver-*

nal equinox. The $\hat{\mathbf{i}}_2$ axis completes the right-handed triad. The epoch used in this work is the current standard epoch (at the time of writing), the $J2000$.

The Local-Vertical/Local-Horizontal (LVLH) frame, also known as the orbit frame, is going to be designated by $O = \{\hat{\mathbf{o}}_1, \hat{\mathbf{o}}_2, \hat{\mathbf{o}}_3\}$. The origin of this frame is attached to the spacecraft. The $\hat{\mathbf{o}}_3$ axis points along the nadir (geocentric) direction, the $\hat{\mathbf{o}}_2$ axis points along the negative orbit normal, and the $\hat{\mathbf{o}}_1$ axis completes the right-handed triad.

The spacecraft body frame $B = \{\hat{\mathbf{b}}_1, \hat{\mathbf{b}}_2, \hat{\mathbf{b}}_3\}$ has its origin fixed on the center of mass of the spacecraft and its axes rotate with the spacecraft. This frame is oriented so that in nominal mode, the payload is nadir pointing, and that under a null pointing error, the B frame is coincident with the O frame. The $\hat{\mathbf{b}}_3$ axis is normal to the payload's face, while the $\hat{\mathbf{b}}_1$ axis is normal to the set of smaller faces of the CubeSat.

2.2. Attitude Dynamics and Kinematics

By considering the body frame B and the ECI frame I presented in Section 2.1, the angular rate of frame B with respect to frame I written in body frame coordinates is going to be denoted by $\vec{\boldsymbol{\omega}} \equiv \vec{\boldsymbol{\omega}}_B^{B/I} = \begin{bmatrix}\omega_1 & \omega_2 & \omega_3\end{bmatrix}^\top$. The kinematic differential equation which translates the relative orientation of frame B with respect to frame I can thus be written in the quaternion form ($\mathbf{q} \equiv \mathbf{q}_I^B$) by [2]

$$\dot{\mathbf{q}} = \frac{1}{2}\boldsymbol{\Omega}(\vec{\boldsymbol{\omega}})\mathbf{q} = \frac{1}{2}\begin{bmatrix} -[\vec{\boldsymbol{\omega}}\times] & \vec{\boldsymbol{\omega}} \\ -\vec{\boldsymbol{\omega}}^\top & 0 \end{bmatrix}\mathbf{q} \tag{1}$$

with

$$[\vec{\boldsymbol{\omega}}\times] = \begin{bmatrix} 0 & -\omega_3 & \omega_2 \\ \omega_3 & 0 & -\omega_1 \\ -\omega_2 & \omega_1 & 0 \end{bmatrix} \tag{2}$$

The dynamic equation of motion of the ORCASat (under the rigid body assumption) is [3]:

$$\mathbf{J}\dot{\vec{\boldsymbol{\omega}}} = (\mathbf{J}\vec{\boldsymbol{\omega}} + \vec{\mathbf{h}}^s) \times \vec{\boldsymbol{\omega}} - \dot{\vec{\mathbf{h}}}^s + \vec{\boldsymbol{\tau}}_B^{perturb} + \vec{\mathbf{u}} \tag{3a}$$

$$\vec{\mathbf{h}}^s = -J^s\omega^s\hat{\mathbf{b}}_2 \quad \text{and} \quad \dot{\vec{\mathbf{h}}}^s = -J^s\dot{\omega}^s\hat{\mathbf{b}}_2 \tag{3b}$$

where $\mathbf{J}$ is the inertia matrix of the CubeSat (including the momentum wheel) about its center of mass, J^s is the principal moment of inertia of the momentum wheel about its spin axis $-\hat{\mathbf{b}}_2$, $\vec{\mathbf{h}}^s$ is the angular momentum of the momentum wheel about its spin axis due to its angular velocity ω^s relatively to the body frame, and $\vec{\boldsymbol{\tau}}_B^{perturb}$ and $\vec{\mathbf{u}}$ are the disturbance torque and the control torque about the system's center of mass in body frame coordinates.

2.3. Linearized Attitude Dynamics and Kinematics

The linear approximation of the nonlinear equations of motion is used in the design of the Linear Quadratic Regulator (LQR) controllers. The linearization is going to be performed about $\mathbf{q}_{e_{ref}} \equiv \mathbf{q}_{O_{ref}}^B = \begin{bmatrix}0 & 0 & 0 & 1\end{bmatrix}^\top$ and $\vec{\boldsymbol{\omega}}_{e_{ref}} \equiv \vec{\boldsymbol{\omega}}_{B_{ref}}^{B/O} = \begin{bmatrix}0 & 0 & 0\end{bmatrix}^\top$. The angular velocity of the spacecraft with respect to the orbit frame O is $\vec{\boldsymbol{\omega}}_e = \begin{bmatrix}\delta\omega_1 & \delta\omega_2 & \delta\omega_3\end{bmatrix}^\top + \vec{\boldsymbol{\omega}}_{e_{ref}} = \delta\vec{\boldsymbol{\omega}}$, while the rotation error between frame B and frame O is $\mathbf{q}_e = \delta\mathbf{q} \otimes \mathbf{q}_{e_{ref}} = \delta\mathbf{q}$ with $\delta\mathbf{q} = \begin{bmatrix}e_1 \sin\frac{\delta\theta}{2} & e_2 \sin\frac{\delta\theta}{2} & e_3 \sin\frac{\delta\theta}{2} & \cos\frac{\delta\theta}{2}\end{bmatrix}^\top \simeq \begin{bmatrix}\delta\theta_1/2 & \delta\theta_2/2 & \delta\theta_3/2 & 1\end{bmatrix} = \begin{bmatrix}\delta\vec{\mathbf{q}}^\top & 1\end{bmatrix}^\top$. By defining the system state as

$$\mathbf{x} = \begin{bmatrix}\delta\omega_1 & \delta\omega_2 & \delta\omega_3 & \delta q_1 & \delta q_2 & \delta q_3\end{bmatrix}^\top \tag{4}$$

The linearized model is given by

$$\dot{\mathbf{x}} = \boldsymbol{A}\mathbf{x} + \begin{bmatrix}\mathbf{J}^{-1}\vec{\mathbf{u}} \\ \mathbf{0}_{3\times 3}\end{bmatrix} \tag{5a}$$

$$\vec{\mathbf{u}} = \vec{\mathbf{m}}_{ctrl} \times \vec{\mathbf{B}}_O \tag{5b}$$

where $\vec{\mathbf{m}}_{ctrl}$ is the dipole moment generated by the magnetorquers, $\vec{\mathbf{B}}_O$ in the local geomagnetic field in frame O and $\mathbf{J} = \text{diag}\begin{pmatrix}J_1 & J_2 & J_3\end{pmatrix}$. The state matrix $\boldsymbol{A}$ is given by

$$\boldsymbol{A} = \begin{bmatrix}\boldsymbol{A}_{11} & \boldsymbol{A}_{12} \\ \boldsymbol{A}_{21} & \boldsymbol{A}_{22}\end{bmatrix} \tag{6a}$$

$$\boldsymbol{A}_{11} = \begin{bmatrix} 0 & 0 & w_0\left(1 - K_x\right) - \frac{h^s}{J_1} \\ 0 & 0 & 0 \\ \frac{h^s}{J_3} - \omega_0\left(1 + K_z\right) & 0 & 0 \end{bmatrix} \tag{6b}$$

$$\boldsymbol{A}_{12} = \begin{bmatrix} -2\omega_0\left(\omega_0 K_x + \frac{h^s}{J_1}\right) & 0 & 0 \\ 0 & 0 & 0 \\ 0 & 0 & 2\omega_0\left(\omega_0 K_z - \frac{h^s}{J_3}\right) \end{bmatrix} \tag{6c}$$

$$\boldsymbol{A}_{21} = \text{diag}\begin{pmatrix}[1/2 & 1/2 & 1/2]\end{pmatrix}, \quad \boldsymbol{A}_{22} = \mathbf{0}_{3\times 3} \tag{6d}$$

where $K_x = (J_2 - J_3)/J_1$, $K_z = (J_1 - J_2)/J_3$, $h^s = J^s\omega^s$, and $\omega_0 = 2\pi/T_{orb}$ is the orbital rate.

3. Attitude Determination Algorithms

In this section, the different algorithms used to directly or indirectly estimate the attitude of the ORCASat are presented.

3.1. Quaternion Estimator (QUEST)

Wahba's problem tries to find the orthogonal matrix $\mathbf{A}$ with determinant +1 that minimizes the cost function [2]

$$J(\mathbf{A}) = \frac{1}{2}\sum_{i=1}^{N} a_i \left\| \vec{\mathbf{b}}_i - \mathbf{A}\vec{\mathbf{r}}_i \right\|^2 \tag{7}$$

This least squares formula tries to find the best fit for the attitude matrix $\mathbf{A}$ given the set of N independent unit vectors $\vec{\mathbf{b}}_i$ measured in the spacecraft's body frame, and the corresponding unit vectors $\vec{\mathbf{r}}_i$ given in the reference frame. The scalar values a_i are non-negative weights. Using the quaternion attitude parametrization instead, Eq. (7) is rewritten as

$$J(\mathbf{q}) = \lambda_0 - \mathbf{q}^\top\mathbf{K}\mathbf{q} \tag{8}$$

where $\lambda_0 = \sum_{i=1}^{N} a_i$, and $\mathbf{K}$ is a symmetric traceless matrix. The cost function from Equation (8) is minimized if $\mathbf{q}^\top \mathbf{K}\mathbf{q}$ is maximized. It can be shown [2] that the attitude quaternion that maximizes $\mathbf{q}^\top \mathbf{K}\mathbf{q}$ is the normalized eigenvector of $\mathbf{K}$ that corresponds to the largest eigenvalue. The QUEST algorithm tries to solve Wahba's problem without solving the eigenvalue/eigenvector problem explicitly. In the case of only two vector observations, there is a closed-form solution for the attitude quaternion given by [2]

$$\mathbf{q} = \begin{cases} \dfrac{1}{2\sqrt{\gamma(\gamma+\alpha)\left(1+\vec{\mathbf{b}}_3\cdot\vec{\mathbf{r}}_3\right)}} \begin{bmatrix} (\gamma+\alpha)\left(\vec{\mathbf{b}}_3\times\vec{\mathbf{r}}_3\right)+\beta\left(\vec{\mathbf{b}}_3+\vec{\mathbf{r}}_3\right) \\ (\gamma+\alpha)\left(1+\vec{\mathbf{b}}_3\cdot\vec{\mathbf{r}}_3\right) \end{bmatrix}, & \alpha \geqslant 0 \\ \dfrac{1}{2\sqrt{\gamma(\gamma-\alpha)\left(1+\vec{\mathbf{b}}_3\cdot\vec{\mathbf{r}}_3\right)}} \begin{bmatrix} \beta\left(\vec{\mathbf{b}}_3\times\vec{\mathbf{r}}_3\right)+(\gamma-\alpha)\left(\vec{\mathbf{b}}_3+\vec{\mathbf{r}}_3\right) \\ \beta\left(1+\vec{\mathbf{b}}_3\cdot\vec{\mathbf{r}}_3\right) \end{bmatrix}, & \alpha < 0 \end{cases} \tag{9}$$

where $\vec{\mathbf{b}}_3$, $\vec{\mathbf{r}}_3$, α, β and γ are given respectively by

$$\vec{\mathbf{b}}_3 = \frac{\vec{\mathbf{b}}_1\times\vec{\mathbf{b}}_2}{\left\|\vec{\mathbf{b}}_1\times\vec{\mathbf{b}}_2\right\|}, \quad \vec{\mathbf{r}}_3 = \frac{\vec{\mathbf{r}}_1\times\vec{\mathbf{r}}_2}{\|\vec{\mathbf{r}}_1\times\vec{\mathbf{r}}_2\|} \tag{10}$$

$$\begin{aligned} \alpha = &\left(1+\vec{\mathbf{b}}_3\cdot\vec{\mathbf{r}}_3\right)\left(a_1\vec{\mathbf{b}}_1\cdot\vec{\mathbf{r}}_1+a_2\vec{\mathbf{b}}_2\cdot\vec{\mathbf{r}}_2\right) \\ &+\left(\vec{\mathbf{b}}_3\times\vec{\mathbf{r}}_3\right)\cdot\left(a_1\vec{\mathbf{b}}_1\times\vec{\mathbf{r}}_1+a_2\vec{\mathbf{b}}_2\times\vec{\mathbf{r}}_2\right) \end{aligned} \tag{11}$$

$$\beta = \left(\vec{\mathbf{b}}_3+\vec{\mathbf{r}}_3\right)\cdot\left(a_1\vec{\mathbf{b}}_1\times\vec{\mathbf{r}}_1+a_2\vec{\mathbf{b}}_2\times\vec{\mathbf{r}}_2\right) \tag{12}$$

$$\gamma = \sqrt{\alpha^2+\beta^2} \tag{13}$$

When $\vec{\mathbf{b}}_3\cdot\vec{\mathbf{r}}_3 = -1$, Equation (9) does not have a solution. This problem can be solved by using the Method of Sequential Rotations (MSR), solving Eq. (9) in a rotated reference frame I_k, multiplying the reference vectors $\vec{\mathbf{r}}_1$ and $\vec{\mathbf{r}}_2$ by $\mathbf{A}_I^{I_k}$. The 180° rotation $\mathbf{A}_I^{I_k}$ about the k'th axis of I gives

$$(\vec{\mathbf{b}}_3\cdot\vec{\mathbf{r}}_3^{\,rotated}) = 2(\vec{\mathbf{b}}_3)_k(\vec{\mathbf{r}}_3^{\,unrotated})_k - \vec{\mathbf{b}}_3\cdot\vec{\mathbf{r}}_3^{\,unrotated} \tag{14}$$

where $(\vec{\mathbf{b}}_3)_k$ and $(\vec{\mathbf{r}}_3^{\,unrotated})_k$ are the k'th components of vectors $\vec{\mathbf{b}}_3$ and $\vec{\mathbf{r}}_3^{\,unrotated}$. From Eq. (14), it is possible to see that if $(\vec{\mathbf{b}}_3\cdot\vec{\mathbf{r}}_3^{\,unrotated})$ is greater than any of the other products $(\vec{\mathbf{b}}_3)_k\cdot(\vec{\mathbf{r}}_3^{\,unrotated})_k$, there is no need for a rotation, otherwise, in order to ensure the greater value for $(\vec{\mathbf{b}}_3\cdot\vec{\mathbf{r}}_3^{\,rotated})$, a rotation is performed about the k'th axis where the value of $(\vec{\mathbf{b}}_3)_k\cdot(\vec{\mathbf{r}}_3)_k$ is greater. The solution $\mathbf{q}_{I_k}^B$ is then rotated back to the original frame: $\mathbf{q}_I^B = \mathbf{q}_{I_k}^B\otimes\mathbf{q}_I^{I_k}$.

3.2. Multiplicative Extended Kalman Filter

The great advantage of the MEKF is the use of the multiplicative quaternion error formulation given by

$$\delta\mathbf{q} = \mathbf{q}\otimes\hat{\mathbf{q}}^{-1} \tag{15}$$

where $\mathbf{q}$ is the attitude quaternion and $\hat{\mathbf{q}}$ is the estimated attitude quaternion. The development of this filter follows from references [2, 4]. The objective of the MEKF is to estimate the error $\delta\mathbf{q}$ and use it to update the propagated attitude quaternion $\hat{\mathbf{q}}$. The linearized model for the propagation of $\delta\mathbf{q}$ is given by

$$\dot{\delta\vec{\mathbf{q}}} = -[\hat{\boldsymbol{\omega}}\times]\delta\vec{\mathbf{q}} + \frac{1}{2}\Delta\vec{\boldsymbol{\omega}} \tag{16a}$$

$$\dot{\delta q_4} = 0 \tag{16b}$$

where $\hat{\boldsymbol{\omega}}$ is the estimated angular velocity of the CubeSat and $\Delta\vec{\boldsymbol{\omega}} = \vec{\boldsymbol{\omega}} - \hat{\boldsymbol{\omega}}$. The first-order approximation assumes that the error quaternion is very small with $\delta q_4 \simeq 1$ constant, being the estimated attitude quaternion close to the true quaternion and allowing to reduce the order of the system by one state. Equation (16a) is going to be re-written using the small-angle approximation $\delta\vec{\mathbf{q}} = \delta\vec{\boldsymbol{\theta}}/2$, yielding

$$\dot{\delta\vec{\boldsymbol{\theta}}} = -[\hat{\boldsymbol{\omega}}\times]\delta\vec{\boldsymbol{\theta}} + \Delta\vec{\boldsymbol{\omega}} \tag{17}$$

The angular velocity $\vec{\boldsymbol{\omega}}$ will be measured using gyroscope sensors. The sensor model, assuming a three-axis rate-integrating gyro, is given by the first-order Markov process:

$$\vec{\boldsymbol{\omega}}(t) = \bar{\boldsymbol{\omega}}(t) - \vec{\boldsymbol{\beta}}(t) - \vec{\boldsymbol{\eta}}_v(t) \tag{18a}$$

$$\dot{\vec{\boldsymbol{\beta}}}(t) = \vec{\boldsymbol{\eta}}_u(t) \tag{18b}$$

where $\bar{\boldsymbol{\omega}}(t)$ is the measured angular velocity, $\vec{\boldsymbol{\beta}}(t)$ is the gyro bias, and $\vec{\boldsymbol{\eta}}_v(t)$ and $\vec{\boldsymbol{\eta}}_u(t)$ are zero-mean Gaussian white-noise processes with spectral densities given by $\sigma_v\mathbf{I}_3$ and $\sigma_u\mathbf{I}_3$ respectively, where $\mathbf{I}_3$ is the identity matrix. The parameters σ_v and σ_u are known as the Angle Random Walk (ARW) and Rate Random Walk (RRW) respectively. The error angular velocity $\Delta\vec{\boldsymbol{\omega}}$ can now be written as $\Delta\vec{\boldsymbol{\omega}} = -\Delta\vec{\boldsymbol{\beta}} - \vec{\boldsymbol{\eta}}_v$, with $\Delta\vec{\boldsymbol{\beta}} = \vec{\boldsymbol{\beta}} - \hat{\vec{\boldsymbol{\beta}}}$. The bias error $\Delta\vec{\boldsymbol{\beta}}$ together with the quaternion error $\delta\vec{\boldsymbol{\theta}}$ will make the new state vector $\mathbf{x} = \begin{bmatrix}\delta\vec{\boldsymbol{\theta}}^\top & \Delta\vec{\boldsymbol{\beta}}^\top\end{bmatrix}^\top$ to be estimated and whose dynamics are given by

$$\dot{\mathbf{x}} = \begin{bmatrix}\dot{\delta\vec{\boldsymbol{\theta}}} \\ \dot{\Delta\vec{\boldsymbol{\beta}}}\end{bmatrix} = \begin{bmatrix}-[\hat{\boldsymbol{\omega}}\times]\delta\vec{\boldsymbol{\theta}} - \Delta\vec{\boldsymbol{\beta}} - \vec{\boldsymbol{\eta}}_v \\ \vec{\boldsymbol{\eta}}_u\end{bmatrix} \tag{19}$$

The estimated state $\hat{\mathbf{x}} = E\{\mathbf{x}\} = \mathbf{0}_6$, since, by definition (Equation (15)), $\delta\hat{\mathbf{q}} = E\{\delta\mathbf{q}\} = \hat{\mathbf{q}}\otimes\hat{\mathbf{q}}^{-1} = \begin{bmatrix}\vec{\mathbf{0}}_3^\top & 1\end{bmatrix}^\top \Rightarrow \delta\hat{\boldsymbol{\theta}} = \vec{\mathbf{0}}$ and $\Delta\hat{\boldsymbol{\beta}} = \hat{\boldsymbol{\beta}} - \hat{\boldsymbol{\beta}} = \vec{\mathbf{0}}$. The dynamics of the estimated state $\hat{\mathbf{x}}$ are then $\dot{\hat{x}} = \mathbf{0}_6$. This result is the key feature of the MEKF. The MEKF propagates the global variables to the time of the next representation, while the error variables (defined by state $\mathbf{x}$) do not need to be propagated because they are identically zero over the propagation step. The update stage updates the error variables which will then be used to update the global variables $\mathbf{q}$ and $\vec{\boldsymbol{\beta}}$. The MEKF error model can thus be written as

$$\dot{\boldsymbol{\epsilon}}^-(t) = \mathbf{F}(t)\boldsymbol{\epsilon}^-(t) + \mathbf{G}(t)\mathbf{w}(t) \tag{20}$$

where $\boldsymbol{\epsilon}^-(t) = \mathbf{x} - \hat{\mathbf{x}}^- = \begin{bmatrix}\delta\vec{\boldsymbol{\theta}}^\top & \Delta\vec{\boldsymbol{\beta}}^\top\end{bmatrix}^\top$ and $\mathbf{w}(t) = \begin{bmatrix}\vec{\boldsymbol{\eta}}_v^\top & \vec{\boldsymbol{\eta}}_u^\top\end{bmatrix}^\top$. The superscript $-$ indicates pre-update variables. The dynamics and process noise distribution matrices $\mathbf{F}(t)$ and $\mathbf{G}(t)$ are given respectively by

$$\mathbf{F}(t) = \begin{bmatrix}-[\hat{\boldsymbol{\omega}}(t)\times] & -\mathbf{I}_3 \\ \mathbf{0}_{3\times3} & \mathbf{0}_{3\times3}\end{bmatrix}, \quad \mathbf{G}(t) = \begin{bmatrix}-\mathbf{I}_3 & \mathbf{0}_{3\times3} \\ \mathbf{0}_{3\times3} & \mathbf{I}_3\end{bmatrix} \tag{21}$$

The covariance matrix of $\mathbf{w}(t)$ is given by

$$\mathbf{Q} = \begin{bmatrix}\sigma_v^2\mathbf{I}_3 & \mathbf{0}_{3\times3} \\ \mathbf{0}_{3\times3} & \sigma_u^2\mathbf{I}_3\end{bmatrix} \tag{22}$$

From here on the development of this filter follows from the standard EKF formulation using the error model from Equation (20), namely the determination of the updated covariance matrix $\mathbf{P}_k^+$ and the determination of the Kalman gain matrix $\mathbf{K}_k$. Given the updated state variables $\delta\hat{\boldsymbol{\theta}}^+$ and $\Delta\vec{\boldsymbol{\beta}}^+$, the update of the estimated gyro bias and angular velocity is given by

$$\hat{\boldsymbol{\beta}}_k^+ = \hat{\boldsymbol{\beta}}_k^- + \Delta\vec{\boldsymbol{\beta}}_k^+ \tag{23}$$

$$\hat{\boldsymbol{\omega}}_k^+ = \bar{\omega} - \hat{\boldsymbol{\beta}}_k^+ \tag{24}$$

while the update of the global attitude representation, the attitude quaternion $\hat{\mathbf{q}}_k^+$, is given by

$$\hat{\mathbf{q}}' = \begin{bmatrix}\frac{1}{2}\delta\hat{\boldsymbol{\theta}}_k^+ \\ 1\end{bmatrix} \otimes \hat{\mathbf{q}}_k^- \tag{25a}$$

$$\hat{\mathbf{q}}_k^+ = \hat{\mathbf{q}}'/\left\|\hat{\mathbf{q}}'\right\| \tag{25b}$$

The observation vector $\vec{\mathbf{y}}_k$ is given by

$$\vec{\mathbf{y}}_k = \vec{\mathbf{h}}(\mathbf{x}_k) + \vec{\mathbf{v}}_k = \mathbf{A}(\mathbf{q})\vec{\mathbf{z}}_I\Big|_{t_k} + \vec{\mathbf{v}}_k \tag{26}$$

$$\mathbf{v}_k \sim \mathcal{N}(0, \mathbf{R}_k) \tag{27}$$

where $\vec{\boldsymbol{z}}_I$ is a measurement unit vector given in frame I by the measurement model, and $\mathbf{R}_k = \sigma_y^2\mathbf{I}_3$ was defined assuming that the measurement errors are isotropic with σ_y corresponding to the noise Standard Deviation (SD) of the sensor. For the update stage described here, only a single measurement was considered. This is not a concern since the MEKF update is linear and so the principle of superposition can be used. The update stage can thus be run repeatedly for each measurement at a time, before the next propagation stage. This is known as Murrell's method. The propagation of $\mathbf{q}$ and $\mathbf{P}$ is done using the discrete propagation technique found in reference [4].

3.3. Magnetometer Calibration Extended Kalman Filter

The magnetometer measurements are going to be modeled as [2]

$$\vec{\mathbf{B}}_{M_k} = (\mathbf{I}_3 + \mathbf{D})^{-1}(\mathcal{O}^\top\mathbf{A}_{R_k}^M\vec{\mathbf{B}}_{R_k} + \vec{\mathbf{b}} + \vec{\boldsymbol{\nu}}_k) \tag{28}$$

where $\vec{\mathbf{B}}_{M_k}$ is the magnetic field measured by the magnetometer at time $t = t_k$, $\vec{\mathbf{B}}_{R_k}$ is the corresponding model of the geomagnetic field in a chosen reference frame such as frame I, $\mathbf{A}_{R_k}^M$ is the unknown rotation matrix of the magnetometer frame M with respect to the reference frame R, $\mathbf{D}$ is a fully-populated matrix of scale factors and non-orthogonality corrections, $\mathcal{O}$ is an orthogonal matrix, $\vec{\mathbf{b}}$ is the magnetometer bias, and $\vec{\boldsymbol{\nu}}_k$ is the measurement noise vector which is assumed to be a zero-mean Gaussian process with covariance $\boldsymbol{\Sigma}_k$. Since the attitude matrix $\mathbf{A}_{R_k}^M$ is unknown, the parameters of $\mathcal{O}$ cannot be determined. The algorithm presented here assumes that $\mathbf{D}$ is symmetric since any skew-symmetric contribution is equivalent to a rotation that can be absorbed in $\mathcal{O}$ [2]. An attitude independent approach is possible by computing

$$y_k = \left\|\vec{\mathbf{B}}_{M_k}\right\|^2 - \left\|\vec{\mathbf{B}}_{R_k}\right\|^2 = h_k(\mathbf{x}) + v_k \tag{29}$$

with $h_k(\mathbf{x})$ and v_k given by

$$\begin{aligned} h_k(\mathbf{x}) = &-\vec{\mathbf{B}}_{M_k}^\top(2\mathbf{D} + \mathbf{D}^2)\vec{\mathbf{B}}_{M_k} + \\ &+2\vec{\mathbf{B}}_{M_k}^\top(\mathbf{I}_3 + \mathbf{D})\vec{\mathbf{b}} - \left\|\vec{\mathbf{b}}\right\|^2 \end{aligned} \tag{30}$$

$$v_k = 2\left[(\mathbf{I}_3 + \mathbf{D})\,\vec{\mathbf{B}}_{M_k} - \vec{\mathbf{b}}\right]^\top\vec{\boldsymbol{\nu}}_k - \|\vec{\boldsymbol{\nu}}_k\|^2 \tag{31}$$

The system state vector $\mathbf{x}$ is defined as

$$\mathbf{x} = \begin{bmatrix}\vec{\mathbf{b}}^\top & \mathbf{D}_v^\top\end{bmatrix}^\top \tag{32a}$$

$$\mathbf{D}_v = \begin{bmatrix}D_{11} & D_{22} & D_{33} & D_{12} & D_{13} & D_{23}\end{bmatrix}^\top \tag{32b}$$

Since the state vector is constant and no noise appears in the state model, $\dot{\mathbf{x}} = \mathbf{0}_9 \Rightarrow \dot{\hat{x}} = \mathbf{0}_9$, meaning that in the propagation stage, the estimated state $\hat{\mathbf{x}}$ will remain constant and equal to the value from the previous update step. From here on, the development of this filter follows from the usual EKF formulation. Lastly, an approximate estimation for the measured magnetic field $\hat{\mathbf{B}}_{M_k}$ can be given by neglecting the effect of $\mathcal{O}$:

$$\hat{\mathbf{B}}_{M_k} = (\mathbf{I}_3 + \hat{\mathbf{D}})\vec{\mathbf{B}}_{M_k} - \hat{\mathbf{b}} \tag{33}$$

where $\hat{\mathbf{B}}_{M_k} \equiv \mathbf{A}_{R_k}^M\vec{\mathbf{B}}_{R_k}$.

4. Attitude Control

In this section, the detumbling controller is presented as well as the four different nadir-pointing attitude controllers studied.

4.1. Detumbling Controller

The detumbling controller implemented in the ORCASat stems from [5]. The control law is given by

$$\vec{\mathbf{m}}_{ctrl} = -\frac{K_d}{\left\|\vec{\mathbf{B}}_B\right\|^2}\vec{\mathbf{B}}_B \times \vec{\boldsymbol{\omega}} \tag{34}$$

where K_d is a positive scalar gain and $\vec{\mathbf{B}}_B$ is the local geomagnetic field given in frame B. Reference [5] also provides a method for computing K_d.

4.2. Sliding Mode Controller

The sliding mode controller implemented in the ORCASat was developed in [6]. Let $\vec{\boldsymbol{\omega}}_e \equiv \vec{\boldsymbol{\omega}}_B^{B/O} = \vec{\boldsymbol{\omega}} - \vec{\boldsymbol{\omega}}_B^{O/I}$ denote the error angular velocity between true angular velocity $\vec{\boldsymbol{\omega}}$ and the desired angular velocity $\vec{\boldsymbol{\omega}}_B^{O/I}$ given in frame B, and $\mathbf{q}_e \equiv \mathbf{q}_O^B = \mathbf{q} \otimes \left(\mathbf{q}_I^O\right)^{-1}$ denote the rotation error between the body frame and the orbit frame. The sliding variable $\vec{\mathbf{s}}$ will be defined as

$$\vec{\mathbf{s}} = \vec{\boldsymbol{\omega}}_e + \boldsymbol{K}\vec{\mathbf{q}}_e \tag{35}$$

where $\boldsymbol{K}$ is a positive definite matrix. In this work, $\boldsymbol{K}$ will be defined as $\boldsymbol{K} = K\mathbf{I}_3$, where K is a positive gain. The desired torque to make the sliding variable $\vec{\mathbf{s}}$ to converge to zero is given by

$$\vec{\boldsymbol{\tau}}_{des} = \vec{\boldsymbol{\tau}}_{eq} - \lambda\vec{\mathbf{s}} \tag{36}$$

$$\begin{aligned}\vec{\boldsymbol{\tau}}_{eq} = &-\left(\mathbf{J}\vec{\boldsymbol{\omega}} + \vec{\mathbf{h}}^s\right) \times \vec{\boldsymbol{\omega}} - \mathbf{J}\left[\vec{\boldsymbol{\omega}}_e\times\right]\mathbf{A}_O^B\vec{\boldsymbol{\omega}}_O^{O/I} \\ &+\mathbf{J}\mathbf{A}_O^B\dot{\vec{\boldsymbol{\omega}}}_O^{O/I} - \frac{1}{2}\mathbf{J}\boldsymbol{K}\left(\vec{\boldsymbol{\omega}}_e q_{e_4} - \vec{\boldsymbol{\omega}}_e \times \vec{\mathbf{q}}_e\right)\end{aligned} \tag{37}$$

where λ is a positive constant number. As explained in [6], the component of the desired control torque which is parallel to the sliding variable $\vec{\mathbf{s}}$ is the only component which is responsible for decreasing the distance of the satellite trajectory to the sliding manifold, therefore, the control torque only needs to compensate for the component of the desired torque which is parallel to $\vec{\mathbf{s}}$. The control law is thus given by

$$\vec{\mathbf{m}}_{ctrl} = \frac{\vec{\mathbf{B}}_B \times \vec{\boldsymbol{\tau}}_{des}^{\parallel}}{\left\|\vec{\mathbf{B}}_B\right\|^2} \tag{38}$$

$$\vec{\boldsymbol{\tau}}_{des}^{\parallel} = \frac{\vec{\boldsymbol{\tau}}_{des}\cdot\vec{\mathbf{s}}}{\left\|\vec{\mathbf{s}}\right\|^2}\vec{\mathbf{s}} = \frac{\vec{\boldsymbol{\tau}}_{eq}\cdot\vec{\mathbf{s}}}{\left\|\vec{\mathbf{s}}\right\|^2}\vec{\mathbf{s}} - \lambda\vec{\mathbf{s}} = \vec{\boldsymbol{\tau}}_{eq}^{\parallel} - \lambda\vec{\mathbf{s}} \tag{39}$$

The control torque produced is $\vec{\mathbf{u}} = \vec{\mathbf{m}}_{ctrl} \times \vec{\mathbf{B}}_B$.

4.3. Linear Quadratic Regulator

The LQR controllers outlined in this section follow from [6]. The magnetic dipole moment $\vec{\mathbf{m}}^{\parallel}$ generated in the direction parallel to the local geomagnetic field vector has no influence in the satellite motion. As such, and following the recommendation encountered in [6], the magnetic dipole moment $\vec{\mathbf{m}}_{ctrl}$ is going to be mapped using a new control signal $\vec{\mathbf{m}}_{cmd}$ according to Equation (40), where the subscript *cmd* stands for commanded dipole moment. This mapping will allow us to obtain a more power efficient controller.

$$\vec{\mathbf{m}}_{cmd} \mapsto \vec{\mathbf{m}}_{ctrl} : \vec{\mathbf{m}}_{ctrl} = \frac{\vec{\mathbf{m}}_{cmd} \times \vec{\mathbf{B}}_B}{\left\|\vec{\mathbf{B}}_B\right\|} \tag{40}$$

Using the new control signal $\vec{\mathbf{m}}_{cmd}$, the control torque $\vec{\mathbf{u}}$ from Equation (5b) can be written as

$$\vec{\mathbf{u}} = \frac{1}{\left\|\vec{\mathbf{B}}_O\right\|}\left[\vec{\mathbf{B}}_O\times\right]\left[\vec{\mathbf{B}}_O\times\right]\vec{\mathbf{m}}_{cmd} \tag{41}$$

where $\vec{\mathbf{B}}_B$ was replaced by $\vec{\mathbf{B}}_O$ according to the development done in Equation (5b). The linear model for the ORCASat, Equation (5a), is then substituted by

$$\dot{\mathbf{x}}(t) = \boldsymbol{A}\mathbf{x}(t) + \boldsymbol{B}(t)\vec{\boldsymbol{u}}(t) \tag{42}$$

with the control vector $\vec{\boldsymbol{u}}(t)$ and the control matrix $\boldsymbol{B}(t)$ given by

$$\vec{\boldsymbol{u}}(t) = \vec{\mathbf{m}}_{cmd}(t) \tag{43}$$

$$\boldsymbol{B}(t) = \begin{bmatrix} \dfrac{\mathbf{J}^{-1}}{\left\|\vec{\mathbf{B}}_O(t)\right\|}\left[\vec{\mathbf{B}}_O(t)\times\right]\left[\vec{\mathbf{B}}_O(t)\times\right] \\ \mathbf{0}_{3\times3} \end{bmatrix} \tag{44}$$

4.3.1 Infinite Horizon Controller

Due to the periodic nature of the geomagnetic field seen from the orbit frame, the linearized model of the satellite can be considered as periodic. It is, however, necessary to find an ideally periodic counterpart of the real geomagnetic field. This is done by averaging the geomagnetic field over $N = 15$ orbits which are contained in a 24h period:

$$\vec{\mathbf{B}}_O^{avg}(t) = \frac{1}{N}\sum_{i=1}^{N}\vec{\mathbf{B}}_O^i(t) \tag{45}$$

where $\vec{\mathbf{B}}_O^i(t)$ is the geomagnetic field of each orbit within the 24h period corresponding to the time interval $t \in [\tau + (i-1)T_{orb}; \tau + iT_{orb}[$. The resultant linear periodic system is given by

$$\dot{\mathbf{x}}(t) = \boldsymbol{A}\mathbf{x}(t) + \hat{\boldsymbol{B}}(t)\vec{\boldsymbol{u}}(t) \tag{46}$$

where $\hat{\boldsymbol{B}}(t)$ is given by Equation (44) after substituting the magnetic field $\vec{\mathbf{B}}_O(t)$ by the magnetic field $\vec{\mathbf{B}}_O^{avg}(t)$ from Equation (45). The control law is then given by [6, 7]

$$\vec{\boldsymbol{u}}(t) = \vec{\mathbf{m}}_{cmd}(t) = -\hat{\boldsymbol{B}}^{\top}(t)\hat{\boldsymbol{P}}(t)\mathbf{x}(t) \tag{47}$$

$$\hat{\boldsymbol{P}}(t) = \sum_{i=0}^{\infty}\boldsymbol{P}_{\infty}(t - iT_{orb}) \tag{48}$$

where, according to [6], the solution $\boldsymbol{P}_{\infty}(t)$ is obtained by solving the differential equation of the following iterative process for an arbitrary final condition:

$$\begin{aligned}\dot{\boldsymbol{P}}_{i+1}(t) = &-\boldsymbol{P}_{i+1}(t)\boldsymbol{A}_i(t) - \boldsymbol{A}_i^{\top}(t)\boldsymbol{P}_{i+1}(t) \\ &-\boldsymbol{K}_i^{\top}(t)\boldsymbol{K}_i(t) - \boldsymbol{Q}(t)\end{aligned} \tag{49}$$

$$\boldsymbol{K}_i(t) = \hat{\boldsymbol{B}}^{\top}(t)\boldsymbol{P}_i(t) \tag{50}$$

$$\boldsymbol{A}_i(t) = \boldsymbol{A} - \hat{\boldsymbol{B}}(t)\boldsymbol{K}_i(t) \tag{51}$$

where $\boldsymbol{Q}(t)$ is a positive semidefinite matrix. The first iteration of Equation (49) is done by solving the regular Differential Riccati Equation (DRE) given by Equation (53) using as final condition $\boldsymbol{P}_{f_1} = \boldsymbol{Q}$. Due to the solution periodicity, the following iteration steps (using Equation (49)) are done using as final condition $\boldsymbol{P}_{f_{i+1}} = \boldsymbol{P}_i(\tau)$. Finally, the control dipole moment $\vec{\mathbf{m}}_{ctrl}$ is obtained from the control vector $\vec{\mathbf{m}}_{cmd}$ according to Equation (40).

4.3.2 Finite Horizon Controller

Instead of using the periodic counterpart of the Earth's magnetic field vector, $\vec{\mathbf{B}}_O^{avg}(t)$, as done is the IHC, the FHC proposes using the real magnetic field. The optimal control vector $\vec{\boldsymbol{u}}(t)$ is then given for each orbit ($t \in [\tau\,;\tau + T_{orb}[$) by

$$\vec{\boldsymbol{u}}(t) = \vec{\mathbf{m}}_{cmd}(t) = -\boldsymbol{B}^\top(t)\boldsymbol{P}(t)\mathbf{x}(t) \tag{52}$$

where $\boldsymbol{P}$ is the solution of the DRE

$$\dot{\boldsymbol{P}}(t) = -\boldsymbol{P}(t)\boldsymbol{A} - \boldsymbol{A}^\top\boldsymbol{P}(t) + \boldsymbol{P}(t)\boldsymbol{B}(t)\boldsymbol{B}(t)^\top\boldsymbol{P}(t) - \boldsymbol{Q}(t) \tag{53}$$

with final condition $\boldsymbol{P}(\tau + T_{orb}) = \boldsymbol{P}_f$. The control dipole moment $\vec{\mathbf{m}}_{ctrl}$ is computed using the control vector $\vec{\mathbf{m}}_{cmd}$ according to Eq. (40). The method for finding $\boldsymbol{P}_f$ is this work consisted of solving the ARE from Equation (56) for $t = \tau + T_{orb}$, i.e., by making $\bar{\boldsymbol{B}} = \boldsymbol{B}(\tau + T_{orb})$ in Eq. (56). The solution obtained for the Riccati matrix, $\boldsymbol{P}_{ARE}$, is then multiplied by a positive scalar gain K : $\boldsymbol{P}_f = K\boldsymbol{P}_{ARE}$.

4.3.3 Constant Gain Controller

The CGC is developed with the aim of avoiding all the necessary computations required by the two previous controllers. The first step of this controller consists of converting the linear periodic time-variant system defined in Eq. (46) to a linear time-invariant system. This is done by averaging the periodic system matrix $\boldsymbol{A}(t)$ and the periodic control matrix $\hat{\boldsymbol{B}}(t)$ for one orbit of period T_{orb} giving

$$\dot{\mathbf{x}}(t) = \bar{\boldsymbol{A}}\mathbf{x}(t) + \bar{\boldsymbol{B}}\vec{\boldsymbol{u}}(t) \tag{54a}$$

$$\bar{\boldsymbol{A}} = \left(\frac{1}{T_{orb}}\int_{\tau}^{\tau+T_{orb}} \boldsymbol{A}(t)dt\right) \tag{54b}$$

$$\bar{\boldsymbol{B}} = \left(\frac{1}{T_{orb}}\int_{\tau}^{\tau+T_{orb}} \hat{\boldsymbol{B}}(t)dt\right) \tag{54c}$$

In the ORCASat case, since the state matrix $\boldsymbol{A}$ is already time-invariant, $\bar{\boldsymbol{A}} = \boldsymbol{A}$. The optimal control vector $\vec{\boldsymbol{u}}(t)$ is then given by

$$\vec{\boldsymbol{u}}(t) = \vec{\mathbf{m}}_{cmd}(t) = -\bar{\boldsymbol{B}}^\top\boldsymbol{P}\mathbf{x}(t) \tag{55}$$

where $\boldsymbol{P}$ is obtained by solving the Algebraic Riccati Equation (ARE):

$$\boldsymbol{P}\bar{\boldsymbol{A}} + \bar{\boldsymbol{A}}^\top\boldsymbol{P} - \boldsymbol{P}\bar{\boldsymbol{B}}\bar{\boldsymbol{B}}^\top\boldsymbol{P} + \boldsymbol{Q} = 0 \tag{56}$$

Finally, the control dipole moment $\vec{\mathbf{m}}_{ctrl}$ is computed according to Equation (40).

5. Results

In this section, the different algorithms of the ADCS will be tested and discussed using the Simulink model of the spacecraft. All results obtained for steady-state were calculated using simulations with a run-time of 24h. All the simulations were performed using the eighth-order Dormand-Prince RK8(7) solver with a fixed time-step of 0.1s. The satellite motion and orbit are influenced by the following perturbations: aerodynamic drag, solar radiation pressure, non-spherical Earth mass distribution, parasitic magnetic torque and gravity gradient torque. The eclipse calculation is done using a ray-sphere intersection method as described in [8]. The sensor models are included, the maximum dipole moment generated by the magnetorquers is $0.25\,\mathrm{A\,m^2}$ in each axis, and the momentum storage of the momentum wheel is $3\mathrm{mN\,m\,s}$ along $-\hat{\mathbf{b}}_2$. All the sensor measurements and the magnetorquers are updated at a rate of 10Hz. The general simulation parameters used are shown in Table 1.

Table 1: General simulation parameters.

Parameters	Value	Unit
Epoch	12:00:00 15/09/2019	UTC
Initial Position (ECI)	$(-4123.994; -2987.433; -4463.062)$	km
Initial Velocity (ECI)	$(6.026; -3.455; -3.263)$	km/s
Orbital period	5549.7	s
Mass of the spacecraft	3.6	kg
Spacecraft inertia matrix (B)	$\mathrm{diag}\begin{pmatrix}0.003 & 0.007 & 0.008\end{pmatrix}$	$\mathrm{kg\,m^2}$
Drag coefficient	2	-
Parasitic dipole moment (B)	$(0.00707; 0; 0.00707)$	$\mathrm{A\,m^2}$
Position of the centroid (B)	$(-4; -2; -2)$	cm
Solar radiation pressure	4.5×10^{-6}	Pa

5.1. Detumbling Controller

The gain used in the detumbling controller is $K_d = 1.21 \times 10^{-5}\mathrm{kg\,m^2\,s^{-1}}$. Two different inertia matrices were used and the attitude estimators were off in these simulations. The initial angular velocity considered is $\vec{\boldsymbol{\omega}}_0 = \begin{bmatrix}0.907 & 0.907 & 0.907\end{bmatrix}(\mathrm{rad\,s^{-1}})$ and the perturbed inertia matrix is $\mathbf{J}_{perturbed} = \begin{bmatrix}0.004410529 & 0.002021869 & 0.000454652\\ 0.002021869 & 0.005932414 & 0.000258699\\ 0.000454652 & 0.0002586989 & 0.007657058\end{bmatrix}$. The performance is measured by the ability of the ADCS to achieve and maintain an angular rate $\|\vec{\boldsymbol{\omega}}\| \leqslant 0.03\mathrm{rad\,s^{-1}}$. The convergence of the controller is shown in Figure 1. The simulations demonstrate that the ADCS can successfully reduce the angular rates and to maintain them below the threshold defined in approximately 1 orbit, even when the inertia tensor is not aligned with frame B.

5.2. Pointing Controller Algorithms

5.2.1 Controllers Comparison, Discussion and Selection

The controllers will be tested using the complete spacecraft Simulink model. The attitude estimation

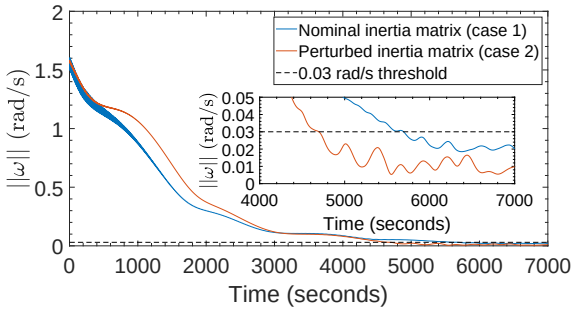

Figure 1: Convergence of the detumbling controller.

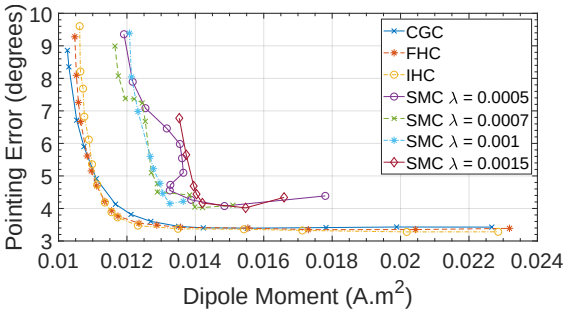

(a) Maximum pointing error.

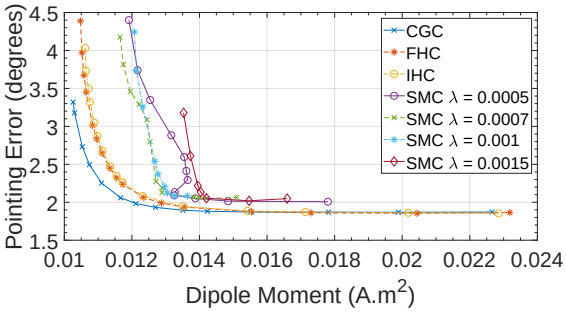

(b) Mean pointing error.

Figure 2: Controllers efficiency comparison.

algorithm, however, does not include the MCEKF. The parameters used in the estimation algorithms are shown in Table 8. It was used in the FHC $K = 1$ and the $\boldsymbol{Q}$ matrix selected for the LQR controllers is $\boldsymbol{Q} = K_Q \operatorname{diag}\left(\begin{bmatrix}1000 & 1000 & 1000 & 1 & 1 & 1\end{bmatrix}\right)$, where the positive gain K_Q is the design parameter. The results are shown in Figures 2a and 2b.

With respect to the maximum error, it can be seen that any of the LQR controllers are more efficient than the best cases for the SMC, i.e, the LQR controllers require less dipole moment than the SMC for the same maximum pointing error. From Figure 2a it is also visible that for smaller pointing errors (less than 5°) the IHC and FHC are slightly more efficient than the CGC, although this difference vanishes when K_Q further increases. For higher errors, the inverse happens. With respect to the mean pointing error, it can be seen that unlike in the previous case, the CGC is the controller which for the same amount of total dipole moment provides the smallest error. In this case, the LQR controllers, once again, have an advantage in terms of efficiency and pointing accuracy in comparison with the SMC. In all cases, the difference between the FHC and the IHC is negligible.

According to the simulations performed, the proposed control algorithm for the ORCASat will be the CGC due to its simpler implementation compared to the IHC and FHC while providing a similar level of performance. The SMC is excluded since it has a clearly worse performance. The gain chosen for the CGC was obtained using $K_Q = 0.7$. The maximum error obtained for this controller is 3.8° and the mean error is 2.0°. The mean total dipole moment used is 0.0121A m^2. This gain was chosen because it provides a low pointing error while not substantially increasing the total dipole moment.

5.2.2 Performance of the ORCASat's controller

The performance of the controller, including the robustness to model uncertainties, will be tested in this section. The controller will be initialized using the four different configurations outlined in Table 2 while the model uncertainties consist of the different cases outlined in Table 3, where $\mathbf{J}_{perturbed}$ is given in Section 5.1. The angular velocity values represent typical detumbling conditions and a higher angular rate condition. The convergence times for the transient analysis without perturbations are shown in Table 4, and the behaviour of the controller is shown in Figure 3a. Table 6 synthesizes the results for the transient analysis under the model uncertainty cases. Figure 3b and Table 5 provide the steady-state analyses results. It is evident that the controller is capable of stabilizing the ORCASat below the 10° threshold, taking less than 0.4 orbits or 35min to do so, even in the presence of the model uncertainties. The degradation of the momentum wheel performance has a significant effect on the steady-state performance of the controller, increasing the maximum error from the base simulation to case 2 and from case 1 to case 3 in 17%.

Table 2: Simulation configurations for the transient analysis of the selected nadir-pointing controller.

Configuration	Initial error	Initial angular velocity $\vec{\omega}_0$ (rad s^{-1})
1	90°	$\begin{bmatrix}6\times10^{-05} & 0.01 & 3\times10^{-05}\end{bmatrix}$
2	180°	$\begin{bmatrix}6\times10^{-05} & 0.01 & 3\times10^{-05}\end{bmatrix}$
3	90°	$\begin{bmatrix}0.05 & 0.05 & -0.05\end{bmatrix}$
4	180°	$\begin{bmatrix}0.05 & 0.05 & -0.05\end{bmatrix}$

5.3. Estimation Algorithms

Four different scenarios were drawn to test the performance of the different algorithms. All the simulations use the full spacecraft Simulink model.

Table 3: Model uncertainty cases for the analysis of the ORCASat's nadir-pointing controller.

Case	Wheel angular mom. (N m s)	Inertia matrix (kg m^2)
1	$\begin{bmatrix}0 & -0.003 & 0\end{bmatrix}$	$\mathbf{J}_{perturbed}$
2	$\begin{bmatrix}0 & -0.002 & 0\end{bmatrix}$	$\mathbf{J}$
3	$\begin{bmatrix}0 & -0.002 & 0\end{bmatrix}$	$\mathbf{J}_{perturbed}$

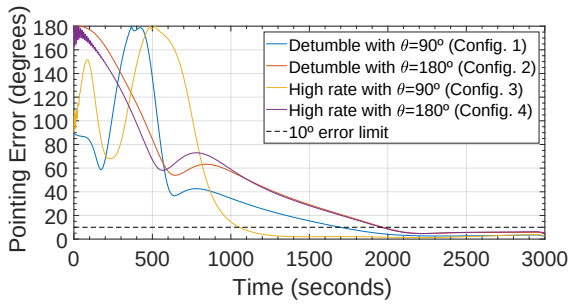

(a) Transient behaviour of the selected controller.

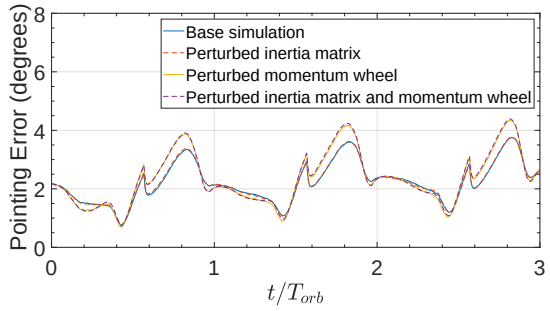

(b) Effect of the model uncertainties on the nominal behaviour of the controller (last 3 orbits of the sim.).

Figure 3: Performance analysis of the ORCASat's nadir-pointing controller.

The simulations also use the chosen controller for the ORCASat. The values used for the bias vector $\vec{\mathbf{b}}$ and for $\mathbf{D}$ in the different scenarios are summarized in Table 7. The parameters used in the different estimators are displayed in Table 8.

5.3.1 Nominal Behaviour of MEKF and QUEST and the Effect of MCEKF

Figure 4a presents the results for the nominal behaviour of the MEKF with and without the effect of the MCEKF in scenario 1. The gray bars shown in the following plots represent the orbit regions where the sun sensors provide data to the estimators. Table 9 provides a synthesis of the results obtained in all the different scenarios. The performance of QUEST in scenario 1 is shown in Figure 4b, using a moving average filter with a window size of 600 samples (1 minute), while Table 10 provides its performance metrics. The MEKF alone did not meet the 2° estimation requirement. The inclusion of the MCEKF allows us to achieve much better results and to meet the estimation requirements, even in the worst-case scenario, scenario 4. Similarly to the case of the MEKF the introduction of the MCEKF significantly improves the accuracy of QUEST. By comparing scenario 1 from Table 9 with Table 10, it is possible to conclude that the MEKF provides better results, both with and without the MCEKF, especially when looking at the maximum error metric. The MEKF is also able to provide attitude knowledge during eclipse while the QUEST algorithm is not. Even with the introduction of the magnetometer calibration filter, the QUEST algorithm cannot satisfy the 2° attitude knowledge requirement, and thus it will only be used for providing an initial attitude quaternion to initialize the MEKF as well as for sanity check.

Table 4: ORCASat pointing controller convergence times (transient case without model uncertainties).

Configuration	Time (s)	Time (t/T_{orb})
1	1697	0.31
2	1969	0.35
3	1055	0.19
4	1957	0.35

Table 5: Performance metrics for the nominal behaviour of the ORCASat's pointing controller.

Case	Max. Error	Mean Error	Dipole Moment
Base sim.	3.82°	1.98°	0.01211A m^2
1	3.76°	1.95°	0.01213A m^2
2	4.47°	2.10°	0.01233A m^2
3	4.40°	2.08°	0.01232A m^2

5.3.2 Transient Behaviour of MEKF and MCEKF and the Effect of QUEST

The convergence of the MEKF will be studied using four different cases. The 1st and 2nd cases will be used to simulate a real-world scenario where the MEKF should acquire the attitude of the ORCASat while in detumbling mode. In the 3rd and 4th cases the simulation will be initialized using a higher angular velocity and no controller will be used to damp those angular rates. These last cases will test the ability of the MEKF to achieve convergence while subjected to a higher angular rate. In cases 1 and 2, the angular rate has a mean magnitude of 0.0029rad s^{-1}, a maximum value of 0.0129rad s^{-1}, and a minimum value of 1.23×10^{-5}rad s^{-1}. In cases 3 and 4, the mean magnitude of the angular velocity is 0.0482rad s^{-1}, the maximum value is 0.0559rad s^{-1}, and the minimum value is 0.0425rad s^{-1}. The initial estimation error for cases 1 and 3 is 90° while for cases 2 and 4, the initial estimation error corresponds to 180°. These errors are initially prescribed about the unit vector $\hat{\mathbf{v}} = \begin{bmatrix}\sqrt{3}/3 & \sqrt{3}/3 & \sqrt{3}/3\end{bmatrix}^\top$, for

Table 6: Convergence times of the ORCASat's pointing controller under the 3 model uncertainty cases.

Configuration	1			2			3			4		
Case	1	2	3	1	2	3	1	2	3	1	2	3
Time (s)	1698	903	901	1967	1965	1965	1056	1675	1732	1962	1983	1987
Time (t/T_{orb})	0.31	0.16	0.16	0.35	0.35	0.35	0.19	0.30	0.31	0.35	0.36	0.36

Table 7: Bias and **D** matrix values used in the different scenarios to test the estimators performance.

Scenario	1	2	3	4
b_1 (nT)	−610	5000	−610	5000
b_2 (nT)	258	3000	258	3000
b_3 (nT)	1793	6000	1793	6000
D_{11}	−0.0438	0.05	−0.0418	−0.0418
D_{22}	−0.1111	0.1	−0.1110	−0.1110
D_{33}	−0.1387	0.05	−0.1334	−0.1334
D_{12}	0.0002	0.05	−0.0778	−0.0778
D_{21}	0.0052	0.05	0.0718	0.0718
D_{13}	0.0161	0.05	−0.0400	−0.0400
D_{31}	0.0002	0.05	−0.0672	−0.0672
D_{23}	−0.0064	0.05	−0.0636	−0.0636
D_{32}	0.0000	0.05	0	0

Table 8: Estimator parameters.

Estimator	Parameter	Value
MEKF	Gyro ARW (σ_v)	$3.493\,08 \times 10^{-8}\,\mathrm{rad\,s^{-1/2}}$
	Gyro RRW (σ_u)	$2.908\,88 \times 10^{-5}\,\mathrm{rad\,s^{-3/2}}$
	TAM SD (σ_m)	$1.5 \times 10^{-5}\,\mathrm{T}$
	Sun Sensor SD (σ_s)	0.5°
QUEST	TAM SD (σ_{mag})	0.029
	Sun Sensor SD (σ_{ss})	0.008
MCEKF	Meas. noise cov. (Σ)	$300\mathbf{I}_3\mathrm{nT}$

Table 9: Performance metrics of the MEKF.

	MCEKF	Scen. 1	Scen. 2	Scen. 3	Scen. 4
Mean Estimation Error (degrees)	Off	1.64	3.05	2.42	5.70
	On	0,21	0,18	0.65	0.67
Max. Estimation Error (degrees)	Off	2.90	5.11	5.11	9.67
	On	0.56	0.52	1.85	1.88

Table 10: QUEST performance metrics in scenario 1 using the moving average filter.

	Mean Error	Maximum Error
MCEKF off	2.04°	8.69°
MCEKF on	0.81°	3.79°

all the cases considered. The initial covariance matrix is $\mathbf{P}_0 = \mathrm{blkdiag}\left(\begin{bmatrix}10\mathbf{I}_3 & \mathbf{I}_3\end{bmatrix} \times 10^{-3}\right)$, where blkdiag denotes a block diagonal matrix. The initial value used for the gyro bias in all the different cases is $\begin{bmatrix}-0.02 & -0.02 & -0.02\end{bmatrix}^\top (\mathrm{rad\,s^{-1}})$,

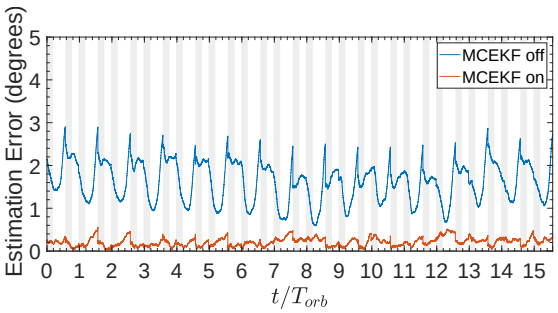

(a) MEKF performance in scenario 1.

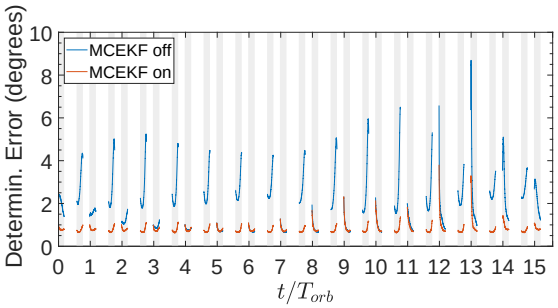

(b) Moving average of the determination error of the QUEST algorithm in scenario 1 with a window size of 600 samples (60s).

Figure 4: Nominal behaviour of the attitude estimators.

corresponding to an initial bias error of $\begin{bmatrix}-0.0271 & -0.0209 & -0.0321\end{bmatrix}^\top (\mathrm{rad\,s^{-1}})$. The evolution of the estimation error for case 2 is shown in Figure 5, while Table 11 provides a summary of the convergence times for all cases. The convergence of the MCEKF will be tested using the values for the magnetometer bias and scale factor and misalignment matrix from scenarios 1 and 4 given by Table 7. These two different sets of values will then be combined with the two different angular velocities from the transient simulations of the MEKF. The MCEKF is initialized with every component of the state vector set to zero. The initial covariance matrix is $\mathbf{P}_0 = \mathrm{blkdiag}\left(\begin{bmatrix}\mathbf{I}_3 & 10^6\mathbf{I}_6\end{bmatrix} \times 10^{-12}\right)$. The MCEKF convergence is shown in Figure 6. Although the MEKF was able to converge in all the cases presented, it can take a relatively long time to do so, up to 4.4 orbits in normal detumble conditions. The use of the QUEST algorithm to initialize the MEKF allows us to reduce those

convergence times to virtually no time. The MCEKF was able to converge in all the cases devised, taking approximately 1 orbit to converge under normal detumbling conditions. In the higher angular rate conditions, the convergence took only approximately 0.15 orbits and it was found that the values of $\vec{\mathbf{b}}$ and $\mathbf{D}$ don't have a visible impact in the convergence times.

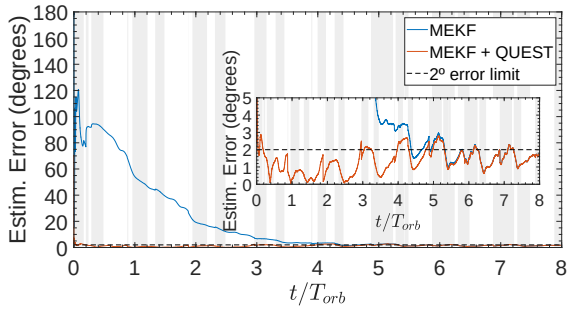

Figure 5: Converngence of the MEKF - detumble mode with 180° initial error (Case 2).

Table 11: MEKF convergence times.

	Time to reach 2° error (t/T_{orb})		Time to reach 2° error (s)	
Case	MEKF	MEKF+QUEST	MEKF	MEKF+QUEST
1	2.36	0.04	13080.8	219.9
2	4.37	0.04	24250.6	219.9
3	2.44	0	13524.4	0
4	6.06	0	33626.9	0

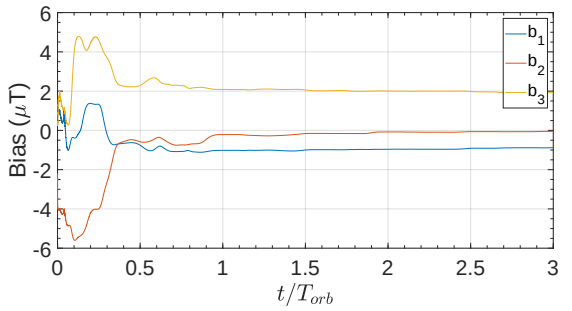

(a) Scenario 1 values under detumbling conditions.

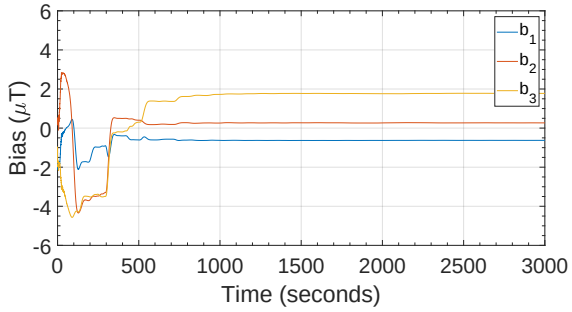

(b) Scenario 1 values under higher angular rates.

Figure 6: Convergence performance of the MCEKF - estimated magnetometer bias vector $\hat{\mathbf{b}}$.

6. Conclusions

From the results shown, it was demonstrated that the proposed ADCS for the ORCASat can successfully accomplish the mission requirements. It was found that the LQR controllers can provide a better pointing accuracy than the sliding mode controller while at the same time using less energy. The CGC selected for the ORCASat was able to achieve a steady-state pointing error smaller than half of the pointing requirement, even in the presence of model uncertainties. The QUEST algorithm was proved useful in decreasing the convergence time of the MEKF from values as high as 4.4 orbits in normal detumbling conditions to less than 5% of the orbital period. The introduction of the MCEKF improved considerably the performance of the MEKF in successfully estimating the attitude of the ORCASat within the proposed requirements. In nominal mode, the maximum estimation error is smaller than 3 times the requirement while the mean estimation error is almost 10 times smaller than the attitude knowledge requirement. The detumbling controller was able to decrease the angular speed of the ORCASat from angular rates as high as $90^\circ\,\mathrm{s}^{-1}$ to less than $2^\circ\,\mathrm{s}^{-1}$ in about 1 orbit.

References

[1] C. S. Agency, "What is a cubesat." `http://www.asc-csa.gc.ca/eng/satellites/cubesat/what-is-a-cubesat.asp`, Last visited on 08/10/2019.

[2] F. L. Markley and J. L. Crassidis, *Fundamentals of spacecraft attitude determination and control*, vol. 33. Springer, 2014.

[3] J. L. Junkins and J. D. Turner, *Optimal spacecraft rotational maneuvers*. Elsevier, 2012.

[4] J. Crassidis and J. Junkins, *Optimal Estimation of Dynamic Systems*. Chapman & Hall/CRC Applied Mathematics & Nonlinear Science, CRC Press, 2011.

[5] G. Avanzini and F. Giulietti, "Magnetic detumbling of a rigid spacecraft," *Journal of Guidance, Control, and Dynamics*, vol. 35, no. 4, pp. 1326–1334, 2012.

[6] R. Wisniewski, *Satellite attitude control using only electromagnetic actuation*. PhD thesis, Aalborg University. Department of Control Engineering, 1996.

[7] D. S. Naidu, *Optimal control systems*. CRC press, 2002.

[8] D. Rondão, "Modelling and simulation of the ecosat-iii attitude determination and control system," Master's thesis, Instituto Superior Técnico, April 2016.